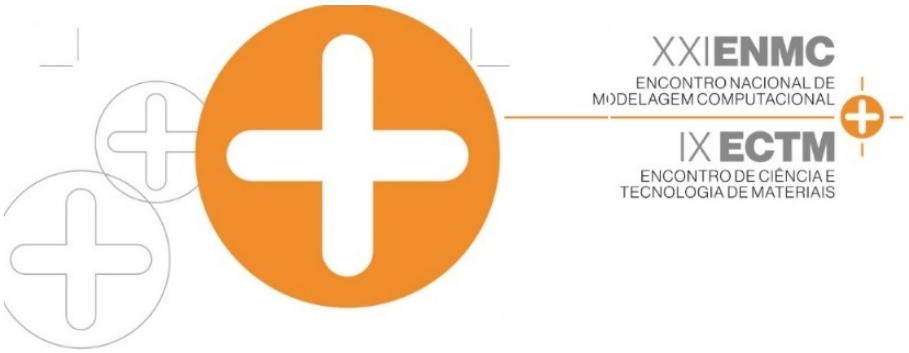

08 a 11 de Outubro de 2018
Instituto Federal Fluminense
Búzios - RJ

A NUMERICAL STRATEGY FOR SPEEDING-UP LARGE-SCALE HEMODYNAMIC SIMULATIONS

Luis Alonso Mansilla Alvarez[1,2] - lalvarez@lncc.br
Pablo Javier Blanco[1,2] - pjblanco@lncc.br
Raúl Antonino Feijóo[1,2] - feij@lncc.br
[1]National Laboratory for Scientific Computing, LNCC/MCTIC, Petrópolis - RJ, Brazil
[2]National Institute of Science and Technology in Medicine Assisted by Scientific Computing, INCT-MACC, Petrópolis - RJ, Brazil

Abstract. *Despite the large medical evidence relating the onset and localization of vascular diseases and flow-related quantities, the massive use of computational models in the daily medical practice is still strongly limited due to the computational burden involved in large-scale hemodynamic simulations. Strategies relying on parallel computing are able to perform some reduction in the computational time of blood flow simulations but, at the same time, the computational resources needed for an effective reduction pose strong limitations, which highlights the need of novel numerical strategies capable to reduce the computational cost of this kind of simulations. In this work, we explore the Transversally Enriched Pipe Element Method (TEPEM) as a novel numerical strategy, specially developed aiming the reduction of both computational time and resources required to perform patient-specific blood-flow simulations. By combining a goal-oriented slab-type geometrical discretization of the vasculature and mixed order polynomials for the field approximation, the TEPEM provides a spatially detailed description of the main flow-related quantities (velocity, pressure, wall shear stress) at a fraction of the cost of approximations based on the classical Finite Element Method (FEM). The potentialities of the presented strategy are studied through numerical examples of increasing complexity scale.*

Keywords: *Hemodynamics, TEPEM, Finite element method, Large-scale simulations*

1. INTRODUCTION

In cardiovascular research, an accurate description of flow-related quantities via computational modeling is a fundamental tool to study the onset and localization of several diseases (Coşkun et al., 2006; Taylor et al., 2013). This evidence motivated the development of several techniques based in the numerical simulation of the blood flow in order to provide an efficient and non-invasive strategy to aid in the prognosis and diagnosis of diseases such as atherosclerosis, while taking in consideration the particularities of each patient-specific geometry.

Among many types of approaches available in the field of computational hemodynamics and considering the potential clinical use of these models, the trade-off between quality of results and computational burden is a key aspect. While full 3D simulations are invaluable to our understanding of hemodynamics quantities and flow patterns, such as recirculation within regions as aneurysms or stenoses, the high computational requirements of time and supercomputing clusters pose real limitations for its use in daily medical practice (Grinberg et al., 2009). On the search of computationally cheaper approaches, dimensionally reduced models (e.g. 1D models) appear to be capable to provide useful information about the global dynamics of the system at a reduced computational cost (Avolio, 1980; Formaggia et al., 2003; Blanco et al., 2014a) but in detriment of a lack of detailed spatial description of important hemodynamic features, such as local flow patterns and transversal dynamics.

In this work, we explore the efficiency of the numerical strategy proposed in (Blanco et al., 2015; Mansilla Alvarez et al., 2017; Mansilla Alvarez, 2018), to deal with the trade-off between accuracy and efficiency presented in current methodologies. The approach, coined as Transversally Enriched Pipe Element Method (TEPEM), is especially aimed for the use in hemodynamics by exploiting some very important characteristics in the cardiovascular system: the pipe-like structure of the domain of interest and the dominant axial dynamics of the blood flow. This method is based on the discretization of the domain of analysis in pipe-type elements, slabs of the tubular domain, for which specific axial and cross-sectional approximation functions are defined. Specifically, physical fields are approximated using a Cartesian product between standard Lagrange polynomial functions of low order for the axial coordinate and high order for transverse coordinates. The combination of the versatility of classical finite element basis functions along the axis combined with an enriched approximation that guarantees accuracy with few degrees of freedom for the transverse direction significantly reduces the size of the algebraic problem, and thus the overall computational cost as well as the computational resources required to execute such simulations.

2. MODEL PROBLEM

Let $\Omega \subset \mathbb{R}^3$ with boundary $\Gamma = \Gamma_i \cup \Gamma_o \cup \Gamma_L$, being Γ_i and Γ_o the inlet and outlet boundaries, respectively. Lateral boundary (the arterial wall) is considered smooth and denoted by Γ_L. Figure 1 presents a geometrical description of the domain of analysis for the fluid flow problem. In this domain, the inlet and outlet boundaries are considered to be flat.

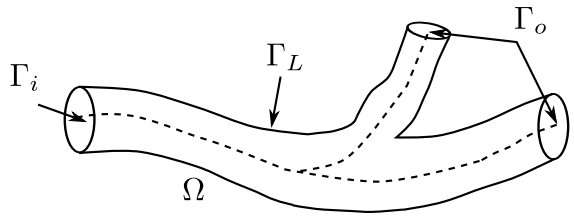

Figure 1- Geometrical description of a typical domain in blood flow simulations.

At inlet and outlet boundaries, conditions of Neumann or Dirichlet type are prescribed. Defective boundary conditions, as for example the prescription of flow rate, are also possible to be imposed through Lagrange multipliers. Once we are interested in simulating the blood flow within a domain corresponding to an isolated region of the cardiovascular system, it is valid to assume that the flow is fully developed at the entrance and exits of this region. This hypothesis

implies in uniform normal component of the traction and null in-plane velocity components. Over the lateral boundary Γ_L no-slip boundary conditions are considered.

Then, the variational formulation for the fluid flow problem reads: find $(\mathbf{u}, p) \in \boldsymbol{\mathcal{V}} \times L^2(\Omega)$ such that

$$\int_\Omega \left[\rho \frac{\partial \mathbf{u}}{\partial t} \cdot \hat{\mathbf{u}} + \rho(\nabla \mathbf{u})\mathbf{u} \cdot \hat{\mathbf{u}} + 2\mu \boldsymbol{\varepsilon}(\mathbf{u}) \cdot \boldsymbol{\varepsilon}(\hat{\mathbf{u}}) - p \operatorname{div} \hat{\mathbf{u}} - \hat{p} \operatorname{div} \mathbf{u}\right] d\Omega = \int_{\Gamma_i} t_i \mathbf{n} \cdot \hat{\mathbf{u}}\, d\Gamma_i + \int_{\Gamma_o} t_o \mathbf{n} \cdot \hat{\mathbf{u}}\, d\Gamma_o \qquad \forall (\hat{\mathbf{u}}, \hat{p}) \in \boldsymbol{\mathcal{V}} \times L^2(\Omega), \tag{1}$$

with ρ and μ being the fluid density and viscosity, respectively, $\boldsymbol{\varepsilon}(\cdot) = (\nabla(\cdot))^S$, $\mathbf{n}$ is the outward normal unit vector and $\hat{(\cdot)}$ denotes an admissible variation of field $(\cdot)$. Space $\boldsymbol{\mathcal{V}}$ is

$$\boldsymbol{\mathcal{V}} = \{\mathbf{u} \in \mathbf{H}^1(\Omega); \mathbf{u}|_{\Gamma_L} = \mathbf{0},\ (\boldsymbol{\Pi}\mathbf{u})|_{\Gamma_i} = \mathbf{0},\ (\boldsymbol{\Pi}\mathbf{u})|_{\Gamma_o} = \mathbf{0}\}, \tag{2}$$

with $\mathbf{H}^1(\Omega) = [H^1(\Omega)]^3$, and where $\boldsymbol{\Pi} = \mathbf{I} - \mathbf{n} \otimes \mathbf{n}$ is the projection operator over the surface whose normal unit vector is $\mathbf{n}$. Finally, t_i and t_o are given data which stand for the magnitude of the normal component of the traction vector imposed at Γ_i and Γ_o, respectively.

3. THE TEPEM STRATEGY

The TEPEM approach is based on the split of the axial and the transversal components of the primal fields in the Navier-Stokes equation: velocity and pressure. The motivation behind this strategy is the a priori knowledge of the blood flow dynamics, which features a dominant direction when circulating through the arterial system. To do this, we perform a very special partitioning strategy associated to an also unusual interpolant choice for the fields.

3.1 Pipe-type mesh discretization

The first ingredient in the TEPEM approach is the meshing strategy to discretize the computational domain. Once our main interest is to model the blood flow into arterial trees, we can consider each domain of analysis as a network of tubular regions. The special tubular structure of the domain allows us to define a geometrical discretization based in tubular finite elements as described next.

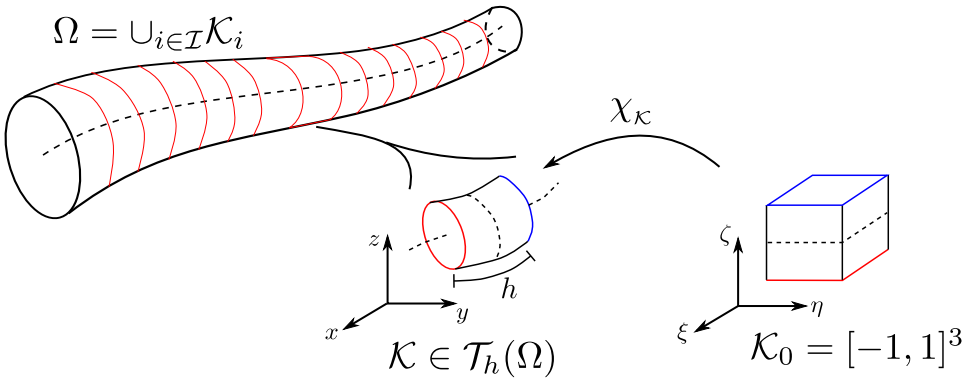

Figure 2- Geometrical mesh formed by pipe-elements for a non-branching domain Ω.

In the scope of TEPEM, the geometry partition consists of pipe elements. This is, the geometric domain Ω is divided into subdomains $\Omega = \cup_{i\in\mathcal{I}}\mathcal{K}_i$ where $\mathcal{K}_i$ denotes a pipe element. Let us denote this partition by $\mathcal{T}_h(\Omega)$ with the mesh parameter h associated to the axial length of the elements. Such particular partition could be obtained by cross-sectional slabbing the domain along the axial direction of the pipe. Each pipe element $\mathcal{K} \in \mathcal{T}_h(\Omega)$ is mapped into the reference element $\mathcal{K}_0 = [-1, 1]^3$ (in the space $\xi\eta\zeta$), through a mapping denoted by $\chi_\mathcal{K}$, and maintaining the axial direction aligned with the ζ-axis. A geometrical description of the mesh structure is presented in Figure 2.

3.2 Transversally enriched field approximation

The interpolation strategy in the TEPEM approach is constructed resorting to the fact that the blood flow is dominantly axial throughout the cardiovascular system. Based on this *a priori* knowledge, we proposed to differentiate the degree of polynomial approximation given to axial and transversal directions for any field, in the reference element $\mathcal{K}_0$. That is, for a defined slab-type partition $\mathcal{T}_h(\Omega)$, we approximate any scalar field w by the function w^h in the finite-dimensional space

$$\mathbb{T}_h^{\mathsf{p},\mathsf{s}} = \left\{ w^h \in L^2(\Omega) : w^h \circ \chi_\mathcal{K}(\xi,\eta,\zeta) = \sum_{j=1}^{\mathsf{s}+1} w_j^{\mathsf{p}}(\xi,\eta)\varphi_j(\zeta), \;\; \mathcal{K} \in \mathcal{T}_h(\Omega) \right\} \tag{3}$$

where $\{\varphi_j : j = 1, \ldots, \mathsf{s}+1\}$ is a basis for the space $\mathbb{P}_\mathsf{s}$ of polynomials up to degree s defined in $\zeta \in [-1, 1]$, and the functions $\{w_j^{\mathsf{p}} : j = 1, \ldots, \mathsf{s}+1\}$ are defined by

$$w_j^{\mathsf{p}}(\xi,\eta) = \sum_{i=1}^{(\mathsf{p}+1)^2} w_{ij}^h \phi_i(\xi,\eta) \qquad j = 1, \ldots, \mathsf{s}+1, \tag{4}$$

with $\{\phi_i : i = 1, \ldots, (\mathsf{p}+1)^2\}$ a basis for the two-dimensional space $\mathbb{P}_\mathsf{p} \times \mathbb{P}_\mathsf{p}$, being $\xi \times \eta \in [-1, 1] \times [-1, 1]$. Axial dependence of the field w, aligned with the axis ζ in the reference element, is approximated through polynomial functions up to order s (axial order) while transversal dependence is approximated by polynomials up to order p (transversal order). The particular case when $\mathsf{s} = \mathsf{p}$ can be understood as a variant of classical pFEM assembled on top of a very specific pipe-element partition.

Our main assumption is that, given a low axial order s, the transversal dynamics can be accurately approximated by employing polynomials of order in the range $4 \leq \mathsf{p} \leq 10$. This allows us to substantially reduce the computational complexity of the problem maintaining reasonably good predictive capabilities.

Once a partition $\mathcal{T}_h(\Omega)$ of $\Omega \subset \mathbb{R}^3$ has been defined, and for a transversal order defined by an even parameter $\mathsf{p} \in \mathbb{N}$, we introduce the finite-dimensional spaces for the velocity and pressure fields

$$\boldsymbol{\mathcal{V}}_h = \left[\mathbb{T}_h^{\mathsf{p},2}\right]^3 \cap C(\overline{\Omega}) \cap \boldsymbol{\mathcal{V}} \qquad \mathcal{Q}_h = \mathbb{T}_h^{\frac{\mathsf{p}}{2},1}. \tag{5}$$

This is, we consider the approximate velocity as being a continuous field, while the pressure is regarded as a discontinuous field. The semi-discrete variational problem becomes: Find

$(\mathbf{u}^h, p^h) \in \boldsymbol{\mathcal{V}}_h \times \mathcal{Q}_h$ such that

$$\int_\Omega \left[\rho \frac{\partial \mathbf{u}^h}{\partial t} \cdot \hat{\mathbf{u}}^h + \rho(\nabla \mathbf{u}^h)\mathbf{u}^h \cdot \hat{\mathbf{u}}^h + 2\mu\boldsymbol{\varepsilon}(\mathbf{u}^h) \cdot \boldsymbol{\varepsilon}(\hat{\mathbf{u}}^h) - p^h \operatorname{div} \hat{\mathbf{u}}^h - \hat{p}^h \operatorname{div} \mathbf{u}^h \right] d\Omega = \int_{\Gamma_i} t_i \mathbf{n} \cdot \hat{\mathbf{u}}^h \, d\Gamma_i + \int_{\Gamma_o} t_o \mathbf{n} \cdot \hat{\mathbf{u}}^h \, d\Gamma_o \qquad \forall (\hat{\mathbf{u}}^h, \hat{p}^h) \in \boldsymbol{\mathcal{V}}_h \times \mathcal{Q}_h. \tag{6}$$

A fully discrete scheme is further obtained by employing an implicit backward Euler scheme for the time discretization and by Picard iterations to linearize the convective term. Regarding the field interpolants, a basis for each discrete space in (5) must be declared. For axial interpolation, classical Lagrangian basis for $\mathbb{P}_2$ is considered for the velocity field while linear Lagrangian basis is considered for the pressure. For the transverse polynomials, the product of two one-dimensional Lagrange polynomials is considered, defined in the coordinates ξ and η. Each function $\phi_i \in \mathbb{P}_\mathsf{p} \times \mathbb{P}_\mathsf{p}$ is defined by

$$\phi_i(\xi, \eta) = \hat{\phi}_j(\xi)\hat{\phi}_k(\eta) \qquad (\xi, \eta) \in [-1, 1]^2 \tag{7}$$

where the indexes i and (j, k) are related through a bijection between the set $\{1, \ldots, (\mathsf{p}+1)^2\}$ and $\{1, \ldots, \mathsf{p}+1\} \times \{1, \ldots, \mathsf{p}+1\}$. Furthermore, the set $\{\hat{\phi}_i, i = 1, \ldots, \mathsf{p}+1\}$ stands for the Lagrange basis functions defined in the set of Chebyshev-Gauss-Lobatto (CGL) nodes, this is, each $\hat{\phi}_i$ is given by

$$\hat{\phi}_i(\xi) = \prod_{n=1, n\neq i}^{\mathsf{p}+1} \frac{\xi - x_n}{x_i - x_n} \qquad i = 1, \ldots, \mathsf{p}+1 \tag{8}$$

where the set $\{x_n : n = 1, \ldots, \mathsf{p}+1\}$ is defined by

$$x_n = -\cos\left(\frac{\pi(n-1)}{\mathsf{p}}\right) \qquad n = 1, \ldots, \mathsf{p}+1 \tag{9}$$

These points are preferred over the natural choice of equidistant distribution of nodes, due to their properties to control the oscillating behavior of high-order interpolants. This problem in the interpolation by high-order polynomials, referred to as *Runge phenomenon*, is graphically presented in Figure 3 as well as a comparison of the interpolated function employing the proposed set of CGL nodes.

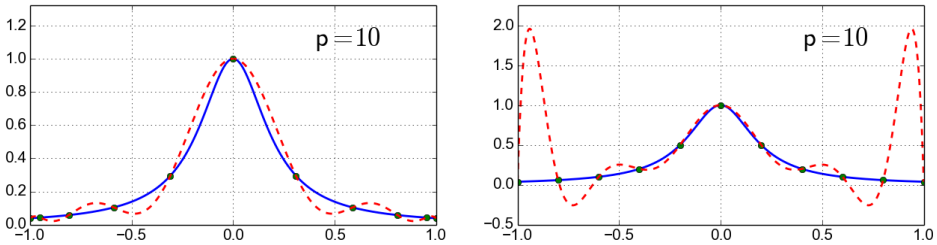

Figure 3- Runge phenomenom: Interpolation of Runge function $f(x) = (1 + 25x^2)^{-1}$ employing CGL nodes (left) and equispaced nodes (right).

4. NUMERICAL RESULTS

In order to demonstrate the capabilities of the TEPEM, in this section the methodology is tested in a synthetic bifurcated domain, a patient-specific left coronary tree and the whole cerebral vasculature described by the one-dimensional ADAN model (Blanco et al., 2014b). The TEPEM solution is compared to a reference solution obtained via standard FEM approximation based on the mini element and SUPG stabilization. Blood properties are set to $\rho = 1.04\,\mathrm{g/cm^3}$ and $\mu = 0.04\,\mathrm{P}$. The system of algebraic equations is solved monolithically using a direct parallel algebraic LU solver for the TEPEM and an iterative GMRES method for the FEM.

4.1 Convergence study in a synthetic carotid artery

The first example is devoted to studying the accuracy properties of the presented strategy. We consider the steady flow of a fluid in a simple bifurcated domain, characterized by a Reynolds number equal to Re = 250. The flow is driven by the imposition of a flow rate at the bottom axial boundary (chosen to ensure the desired Reynolds number), homogeneous Neumann boundary conditions are considered at the outlets and no-slip condition for the velocity is imposed over the lateral surface.

For comparison purposes, a reference solution is obtained simulating the flow via standard FEM in an extremely fine tetrahedral mesh. For the TEPEM, the mesh is composed by 95 pipe-elements and the transversal order considered is in the range $4 \leq \mathrm{p} \leq 12$. The geometry considered in this example, as well as a detailed view of the velocity and pressure distribution, is presented in Figure 4.

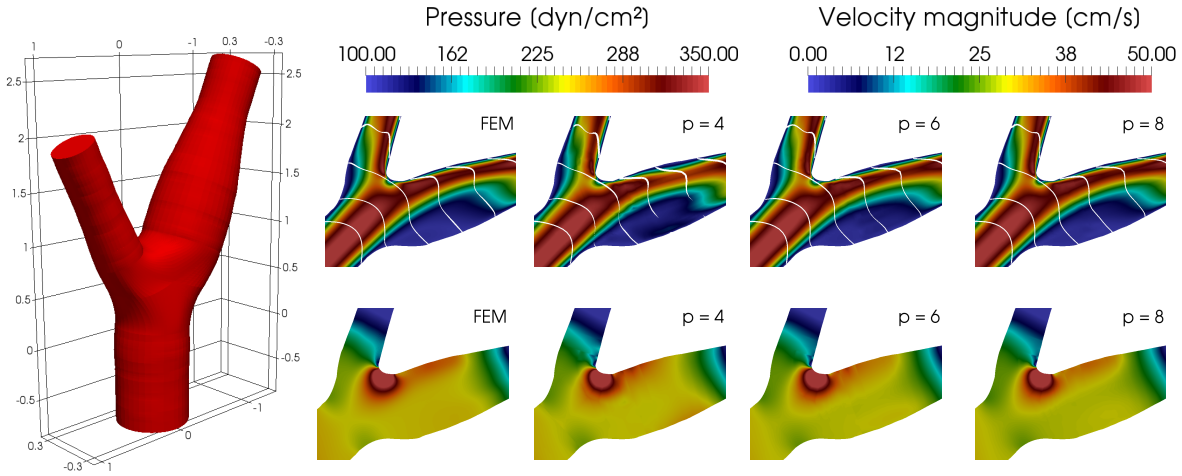

Figure 4- Left: Geometry of the synthetic carotid artery. Right: Comparison of velocity magnitude and pressure field between the FEM reference solution and the TEPEM for different transversal enrichment orders.

The reduction in the computational burden obtained with the TEPEM is clearly perceptible in Table 1, where it is reported a reduction in the number of degrees of freedom up to 90% (compared with the reference solution) and a speeding-up in the wall-clock time between 5 and 800 times. The convergence of the TEPEM, with respect of the transversal order, follows from the velocity and pressure errors presented in Table 1.

Table 1- Top table: Comparison between number of elements, degrees of freedom and computational time (in minutes) to solve the steady state problem with the FEM and the TEPEM approaches. Bottom table: Relative error in the velocity field, in the velocity gradient and in the pressure field between the TEPEM solution and the reference FEM solution.

	FEM	TEPEM				
		$\mathsf{p}=4$	$\mathsf{p}=6$	$\mathsf{p}=8$	$\mathsf{p}=10$	$\mathsf{p}=12$
Elements	12 276 715			95		
DoFs	7 880 372	15 121	29 922	49 729	74 542	104 361
DoFs reduction		99.80%	99.62%	99.36%	99.05%	98.67%
Wall clock time	105.4	0.12	1.04	3.95	13.5	20.7

	TEPEM				
	$\mathsf{p}=4$	$\mathsf{p}=6$	$\mathsf{p}=8$	$\mathsf{p}=10$	$\mathsf{p}=12$
$\|\mathbf{u}_\mathrm{F}-\mathbf{u}_\mathrm{T}\|$	$0.23\cdot10^{-2}$	$0.22\cdot10^{-2}$	$0.10\cdot10^{-2}$	$8.36\cdot10^{-3}$	$5.50\cdot10^{-3}$
$\|\mathbf{u}_\mathrm{F}-\mathbf{u}_\mathrm{T}\|$	$0.69\cdot10^{-2}$	$0.65\cdot10^{-2}$	$0.41\cdot10^{-2}$	$0.37\cdot10^{-2}$	$0.33\cdot10^{-2}$
$\|p_\mathrm{F}-p_\mathrm{T}\|$	$0.21\cdot10^{-2}$	$3.93\cdot10^{-3}$	$3.47\cdot10^{-3}$	$3.05\cdot10^{-3}$	$2.17\cdot10^{-3}$

4.2 Wall shear stress in the right coronary artery

A correct spatial description of the wall shear stress (WSS), which is defined by WSS $= -2\mu(\nabla^s\mathbf{u})\mathbf{n}$, is of utmost importance in the medical practice due its role in the progression of some vascular diseases, such as atherosclerosis. The computation of this index, via classical FEM strategies, demand a mesh refinement near to the surface wall to correctly capture the boundary layers dynamics. On the other hand, in the TEPEM the increase of the transversal order naturally improves the model capabilities to deal with possible (transversal) boundary layers. In this example, we analyze the capabilities of the presented approach in the prediction of the WSS in a patient-specific arterial geometry obtained from computed tomography angiography. The steady flow is simulated considering homogeneous Neumann condition at the inlet, while a flow rate equal to Q = 2 cm^3/s is distributed among the outlets boundaries. The associated Reynolds number results Re = 150 measured at the inlet section.

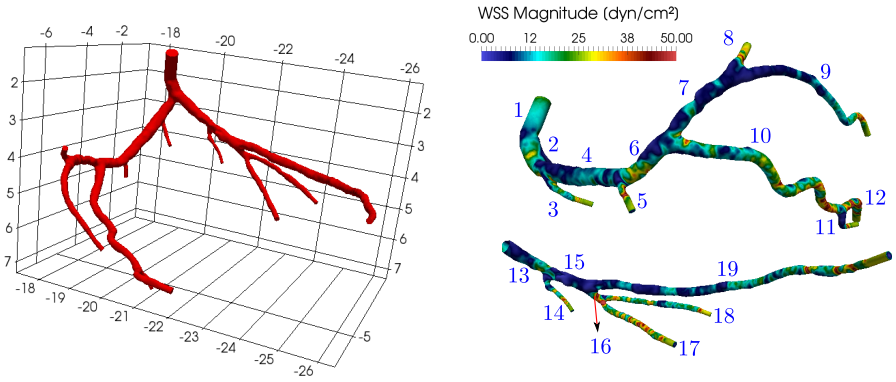

Figure 5- Left: Coronary tree geometry obtained via image segmentation (length units are in centimeters). Right: Spatial distribution of the WSS obtained with FEM in the right (top) and left (bottom) half of the arterial tree. Arterial branches are enumerated for a further detailed comparison between FEM and TEPEM approximation of WSS field.

The FEM simulation is composed by $4\,094\,885$ tetrahedral elements and for which 50 processors are required for its solution. This mesh is similar to that employed in simulations performed routinely. The geometry and the spatial description of the wall shear stress obtained with the FEM are outlined in Figure 5.

For the TEPEM, the pipe mesh is composed by 476 slab elements and 10 processors are employed. The reduction in the computational burden is measured through the inclusion of the *average time* index, defined by multiplying the wall-clock simulation time and the number of processors employed in each case. These values, as well as the degrees of freedom for FEM and TEPEM are displayed in Table 2. As can be seen, reduction in the average computational time is around 200 and 21 times for $\mathsf{p} = 4$ and $\mathsf{p} = 6$, respectively, compared to the typical FEM simulation. The TEPEM, considering the lower values of transversal enrichment considered here $(\mathsf{p} = 4, 6)$, is capable to predict flow structures in close agreement with the FEM solution. The agreement is confirmed when comparing the WSS, as exhibited in Figure 6. The unfolded view of the WSS along the longitudinal axes allows to scrutiny the capabilities of the TEPEM to capture intricate patterns at a fraction of the cost implied by classical FEM simulations.

Table 2- Comparison of the computational burden in the FEM and TEPEM approaches. The cost is evaluated through the average computational time (in minutes), obtained by multiplying the number of processors and the wall-clock time at each simulation, and also through the relative reduction in the number of degrees of freedom.

		FEM	TEPEM			
			$\mathsf{p} = 4$	$\mathsf{p} = 6$	$\mathsf{p} = 8$	$\mathsf{p} = 10$
Elements		4 094 885	476			
DoFs	Total number	2 814 015	78 226	153 469	253 866	379 417
	Relative reduction	-	97.22%	94.54%	90.97%	86.51%
Total time	Average (min)	1 558.85	8.16	74.03	324.82	1 003.05
	Relative reduction	-	99.47%	95.25%	79.16%	35.65%

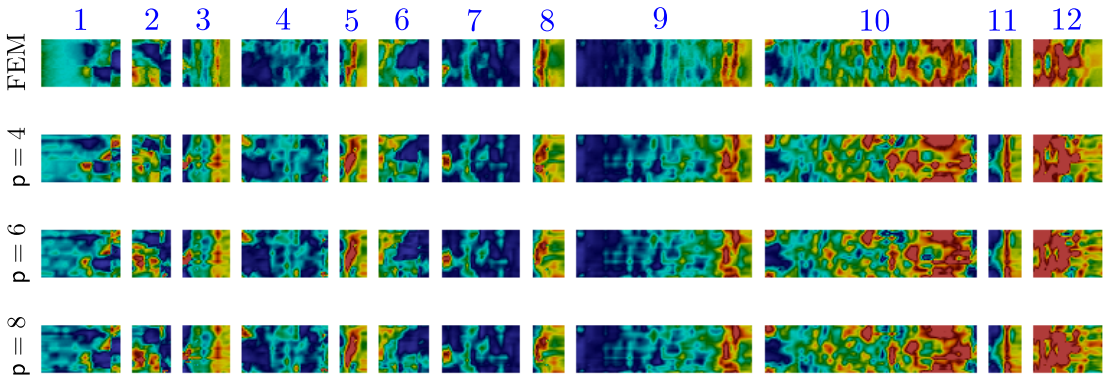

Figure 6- Unfolded view of spatial distribution of WSS over the vessel surface obtained with FEM and with TEPEM for different transversal orders.

4.3 Towards large-scale hemodynamic simulations

To illustrate the application of the TEPEM in a large scale problem, the blood flow in steady-state regime is simulated in the whole intracranial arterial vasculature. The geometry is reconstructed based on the anatomical information provided by the ADAN model (Blanco et al., 2014b), wherein the cerebral vasculature is composed by 126 branches and 64 bifurcations. The flow is driven by the imposition of a total flow equal to $Q = 5$ cm^3/s distributed among the two vertebral and two internal carotid arteries, as seen in Figure 7. Over the outlet boundaries, a resistance-type boundary condition is imposed ($R = 6 \cdot 10^3$ dyn·s·cm^{-5}), such that the blood pressure is in the normal physiological range. Over the lateral surface of the vessel, no-slip boundary conditions are imposed and zero velocity is considered as initial condition.

The blood flow is simulated by discretizing the geometry in $3\,789$ pipe elements, employing a number of processors equal to NP = 60 and transversal polynomial order $\mathsf{p} = 6$. Involving a total of $1\,174\,320$ degrees of freedom, the capabilities of the TEPEM to describe the spatial heterogeneities can be appreciated in Figure 7 where the approximated pressure and WSS fields are presented. Concerning the computational time employed in this simulation, the time to perform a single Picard iteration was 36 seconds, while the total wall-clock time until reaching the steady state solution is around 12 minutes. Clearly, this is a small amount of time in view of the level of information provided by the proposed approach.

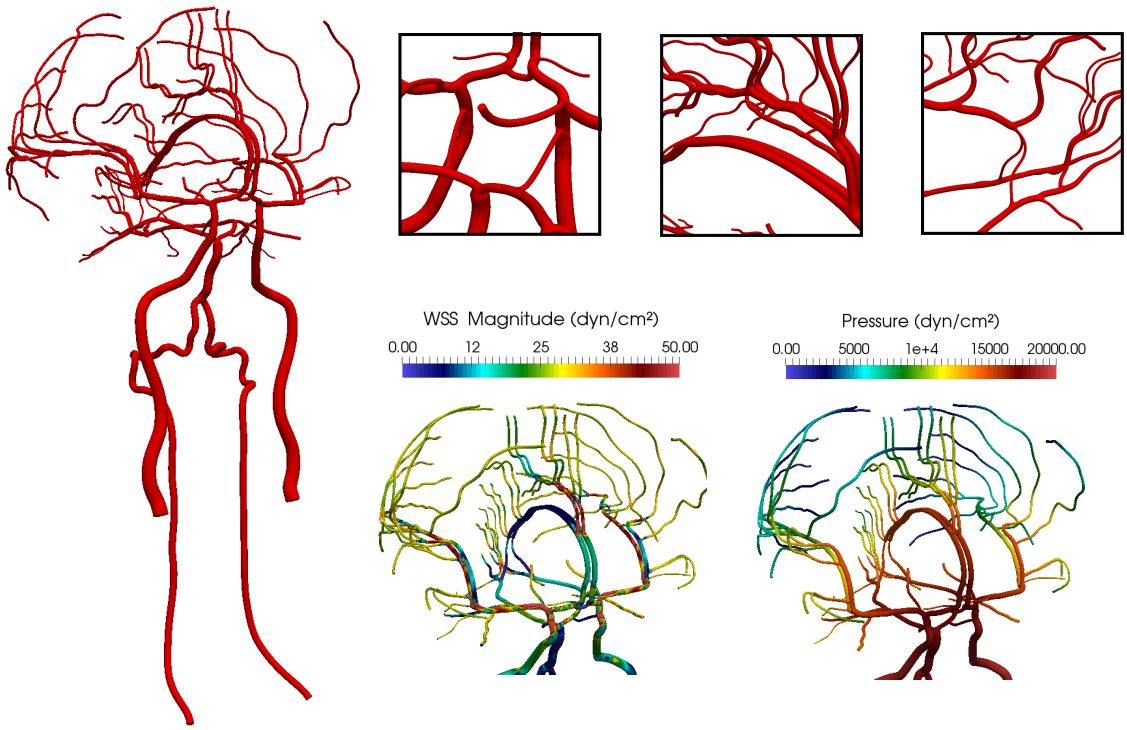

Figure 7- Left: Geometry for the 3D intracranial arterial system reconstructed from the 1D ADAN model. Right top: Detailed view of the geometry. Right bottom: Detail of the spatial variation of pressure and WSS fields obtained with the TEPEM strategy.

5. FINAL REMARKS

The capabilities of the Transversally Enriched Pipe Element Method (TEPEM) were explored in the hemodynamic realm. The basic idea of this methodology is supported by the discriminated utilization of axial and transversal polynomials for the approximation of physical fields, providing a severe reduction in the computational cost, but keeping a reasonable accuracy according to medical needs. Through numerical examples, it has been shown that the TEPEM can become an extremely efficient tool in terms of the trade-off between accuracy and computational cost, delivering excellent predictions at a fraction of the effort required by standard FEM techniques.

Acknowledgments

This work was partially supported by the Brazilian agencies CAPES, CNPq and FAPERJ. The support of these agencies is gratefully acknowledged.

REFERENCES

Avolio, A. (1980). Multi-branched model of the human arterial system. *Med Biol Eng Comput*, 18:709–718.

Blanco, P., Mansilla Alvarez, L., and Feijóo, R. (2015). Hybrid element-based approximation for the Navier–Stokes equations in pipe-like domains. *Comp. Meth. Appl. Mech. Engrg.*, 283:971–993.

Blanco, P., Watanabe, S., Dari, E., Passos, M., and Feijóo, R. (2014a). Blood flow distribution in an anatomically detailed arterial network model: criteria and algorithm. *Biomechecanics and Modeling in Mechanobiology*, 13:1303–1330.

Blanco, P., Watanabe, S., Passos, M., Lemos, P., and Feijóo, R. (2014b). An anatomically detailed arterial network model for one-dimensional computational hemodynamics. *IEEE Trans. Biomed. Eng.*, 62(2):736–753.

Coşkun, A., Chen, C., Stone, P., and Feldman, C. (2006). Computational fluid dynamics tools can be used to predict the progression of coronary artery disease. *Physica A: Statistical Mechanics and its Applications*, 362(1):182–190.

Formaggia, L., Lamponi, D., and Quarteroni, A. (2003). One-dimensional models for blood flow in arteries. *J. Engrg. Math.*, 47(3-4):251–276(26).

Grinberg, L., Anor, T., Madsen, J., Yakhot, A., and Karniadakis, G. (2009). Large-scale simulation of the human arterial tree. *Clin. Exp. Pharmacol. Physiol.*, 36:194–205.

Mansilla Alvarez, L. (2018). *An effective numerical technique for pipe-like domains and its application in computational hemodynamics*. PhD thesis, Laboratório Nacional de Computação Científica - LNCC, Petrópolis - Brazil.

Mansilla Alvarez, L., Blanco, P., Bulant, C., Dari, E., Veneziani, A., and Feijóo, R. (2017). Transversally enriched pipe element method (tepem): An effective numerical approach for blood flow modeling. *Int. J. Num. Meth. Biomed. Engng.*, 33(4).

Taylor, C., Fonte, T., and Min., J. (2013). Computational Fluid Dynamics Applied to Cardiac Computed Tomography for Noninvasive Quantification of Fractional Flow Reserve. *Journal of the American College of Cardiology*, 61(22):2233–2241.